

Lattice vibration as a knob on exotic quantum criticalitySangEun Han^{1,*}, Junhyun Lee^{2,*} and Eun-Gook Moon^{1,†}¹*Department of Physics, Korea Advanced Institute of Science and Technology, Daejeon 34141, Korea*²*Department of Physics, Condensed Matter Theory Center and Joint Quantum Institute, University of Maryland, College Park, Maryland 20742, USA* (Received 28 February 2020; revised 15 November 2020; accepted 20 December 2020; published 21 January 2021)

Control of quantum coherence in a many-body system is one of the key issues in modern condensed matter, and conventional wisdom is that lattice vibration is an innate source of decoherence. Much research has been conducted to eliminate lattice effects. Challenging this wisdom, we show that lattice vibration may not be a decoherence source but an impetus of a novel coherent quantum many-body state. We demonstrate the possibility by studying the transverse-field Ising model on a chain with renormalization group and density-matrix renormalization group methods and theoretically discover a stable $\mathcal{N} = 1$ supersymmetric quantum criticality with central charge $c = 3/2$. Thus, we propose an Ising spin chain with strong spin-lattice coupling as a candidate to observe supersymmetry. Generic precursor conditions of novel quantum criticality are obtained by generalizing the Larkin-Pikin criterion of thermal transitions. Our work provides the perspective that lattice vibration may be a knob for exotic quantum many-body states.

DOI: [10.1103/PhysRevB.103.014435](https://doi.org/10.1103/PhysRevB.103.014435)**I. INTRODUCTION**

Quantum critical systems have been a central area of research because fundamentally new phenomena with enlarged symmetry may emerge from quantum fluctuations, which may also extend to nonzero temperatures [1]. A key feature of quantum critical systems is that their wave function is made up of a complex superposition of configurations at all length scales. Universal scale dependence of correlation functions, characterized by their critical exponents, indicates intrinsic long-range entanglement [2,3]. Such criticalities usually appear at quantum critical points between quantum phases [1], but quantum critical phases also exist, for example, in symmetry-protected topological semimetals [4–7] and superconductors [8,9]. If a quantum critical system is hosted with a lattice structure, then an intrinsic length scale, the lattice constant, exists with broken translational symmetry, and acoustic phonons appear down to the lowest energy scale, guaranteed by the Goldstone theorem.

One important question in quantum critical systems is how gapless quantum critical modes couple to acoustic phonons. Since the two types of excitations are intrinsically gapless, naive perturbative calculations fail, and careful analysis of the interplay between the two modes is necessary. Most of all, it is essential to check whether the two coherent modes remain coherent as a whole once they are coupled. The existence of a coherent quantum critical state with phonons indicates that acoustic phonons do not play the role of a heat bath, which is in drastic contrast to the conventional wisdom that lattice vibration is an innate source of decoherence. Note that it is essential that acoustic phonons are dealt with as dynamical

degrees of freedom to maintain quantum coherence of the whole system.

The coupling physics in a quantum critical system was overlooked for a long time until recent experiments reported that acoustic phonons qualitatively affect the critical behavior, such as scaling exponents of the dielectric susceptibility in quantum ferroelectric materials SrTiO₃ and KTaO₃ [10–13], followed by a theory proposing a new class of criticality from spin-lattice coupling [14] applying the quantum-classical mapping. For the case of classical criticality, where a phase transition occurs at a nonzero temperature, the effect of lattice vibration has been exhaustively studied in the literature. Larkin and Pikin first provided the instability condition for classical critical systems coupled with lattice vibrations in terms of the specific heat critical exponent [15]. Other groups subsequently performed renormalization group (RG) analysis in a variety of critical models and applied the Larkin-Pikin criterion [16–20]. Models with smaller degrees of freedom such as the two- and three-dimensional Ising models become more unstable under lattice vibrations, and first-order phase transitions often appear.

In this work, we demonstrate striking interplay physics between quantum critical modes and acoustic phonons and find quantum critical classes with acoustic phonons. We first analyze the quantum transverse Ising model on a one-dimensional lattice. Surprisingly, although the transverse Ising model and acoustic phonons are both well-studied problems, we uncover the existence of a supersymmetric stable fixed point with central charge $c = 3/2$ at the critical point of the spins. We also predict experimental implications for the measurable phonon velocity, which may serve as a smoking gun for supersymmetry in a condensed-matter system. This exemplifies the possible physics stemming from the interaction between quantum criticality and acoustic phonons.

*These authors contributed equally to this work.

†egmoon@kaist.ac.kr

TABLE I. Scaling dimensions of the coupling ($[g] = 1/\nu - d_{\text{eff}}/2$) in models with continuous phase transitions. The effective dimension $d_{\text{eff}} \equiv (d + 1)$ is introduced for spatial dimension d . For $[g] > 0$, the original criticalities become unstable, signaling the first-order phase transition under lattice vibration, while the criticalities remain stable for $[g] < 0$. For $[g] = 0$, a novel quantum criticality may appear as in the aforementioned spin-chain model.

Model	d_{eff}	ν	$[g]$
Ising [21]	2	1	0
Tricritical Ising [21]	2	5/9	>0
Three- (four-) state Potts [21]	2	5/6 (2/3)	>0
q -state clock ($q > 4$) [22]	2	∞	<0
Ising [23]	3	0.63	>0
q -state clock ($q \geq 4$) [24]	3	0.67	<0
$O(N)$ ($N \geq 2$) [23,24]	3	≥ 0.67	<0
$\mathcal{N} = 2$ WZ SUSY [25]	3	0.917	<0
$\mathcal{N} = 2$ XYZ SUSY [26]	3	$1/2 + \epsilon/4$	<0
$O(N)$ [1]	4	1/2	0

We also study the generic scenario when an order parameter of a continuous quantum phase transition is coupled with the underlying lattice vibration. The stability condition, which may be considered a quantum version of the Larkin-Pikin criterion, is obtained based on the scaling dimension of the coupling. We enumerate the stabilities of quantum critical models using this new criterion (Table I).

The outline of this paper is as follows. In Sec. II, we introduce a model Hamiltonian for the transverse-field Ising model with lattice vibration. The noninteracting lattice Hamiltonian and spin-lattice coupling Hamiltonian are introduced. In Sec. III, we analyze our model at the critical point by using the momentum-shell RG method. The low-energy action at the critical point is explicitly written. We obtain the RG flow equations in terms of the dimensionless parameters and show the existence of a stable fixed point. Also, we find the intriguing property of the stable fixed point, which is the emergence of $\mathcal{N} = 1$ supersymmetry (SUSY). In Sec. IV, we analyze our model by using the numerical method, in particular, the density-matrix renormalization group (DMRG) method. By calculating entanglement entropy, we find the central charge $c = 3/2$, which is consistent with the results of Sec. III, at the stable fixed point. In Sec. V, we generalize our spin chain result into generic quantum criticality with lattice vibrations. From scaling analysis of coupling between generic quantum criticality and lattice vibration, we find the condition for the stability of the generic quantum criticality with lattice vibrations. Section VI presents the discussion and conclusion.

II. MODEL

Let us consider the transverse-field Ising chain model with acoustic phonons for a proof of principle. The Hamiltonian without spin-lattice coupling is [1,27]

$$H_0 = \sum_i \left[-J s_i^x s_{i+1}^x - h s_i^x + \frac{P_i^2}{2M} + \frac{M\omega_0^2}{2} (u_{i+1} - u_i)^2 \right], \quad (1)$$

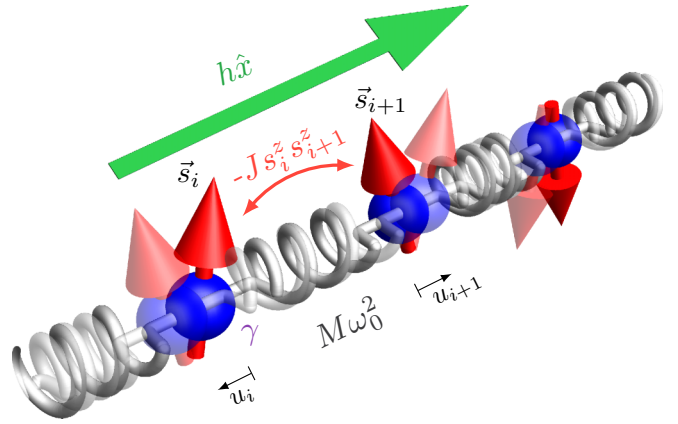


FIG. 1. Illustration of the transverse Ising model under lattice vibrations. The red arrow stands for the Ising spin, and the springs represent the vibrating lattices. The green arrow at the top shows the transverse field, and γ is the coupling constant between the spin degree of freedom and lattice vibrations.

with a magnetic exchange interaction J , a transverse magnetic field h , Debye frequency ω_0 , and ion mass M (Fig. 1). The deviation of spin positions is captured by u_i , and the quantum spins are represented by the Pauli matrices ($s_j^{x,y,z}$) at site j . The Hamiltonian is exactly solvable and discussed extensively in the literature [1,27]. Following the literature, the Hamiltonian is expressed as $H_0 = \sum_k \epsilon_k (f_k^\dagger f_k - \frac{1}{2}) + \omega_k (b_k^\dagger b_k + \frac{1}{2})$. The bosonic operators (b_k, b_k^\dagger) describe acoustic phonons with the energy spectrum, $\omega_k = 2\omega_0 |\sin(\frac{ka}{2})|$, and the fermionic ones (f_k, f_k^\dagger) are from the Jordan-Wigner transformation of spins and have an energy spectrum of $\epsilon_k = 2J\sqrt{1 - 2r \cos(ka)} + r^2$. Lattice spacing a and the ratio $r = h/J$ are introduced. Note that the pure spin term may also be represented by two Majorana fermions at each site [$\eta_j^{(1)} = -(\prod_{i<j} s_i^x) s_j^z$ and $\eta_j^{(2)} = (\prod_{i<j} s_i^x) s_j^y$]. For example, the spin exchange term becomes $s_j^z s_{j+1}^z = -i\eta_j^{(2)} \eta_{j+1}^{(1)}$ in this representation. In Fig. 2(a), the phase diagram of our system is illustrated. At $r = 1$, a gapless Majorana fermion excitation arises in the pure spin model, indicating the Ising universality class of central charge $c = 1/2$. On the other hand, the phonon spectrum is gapless because phonons are Goldstone bosons of translational symmetry.

The spin-lattice coupling appears with spatial modulation of the magnetic exchange interaction, $J \rightarrow J_{i,i+1} = J + \gamma(u_{i+1} - u_i) + O((u_{i+1} - u_i)^2)$ [28], and the leading interaction term is

$$H_1 = \gamma \sum_i (u_{i+1} - u_i) s_i^z s_{i+1}^z. \quad (2)$$

Away from the critical point ($r \neq 1$), the perturbative calculation indicates that the decay rate of a quantum state is, indeed, proportional to $\tau^{-1} \propto \gamma^2$, and the spin-lattice coupling becomes a source of decoherence.

III. SUPERSYMMETRY FROM SPIN-LATTICE COUPLING

Now, let us consider a quantum critical state. The scale invariance allows us to use the critical theory of spin and

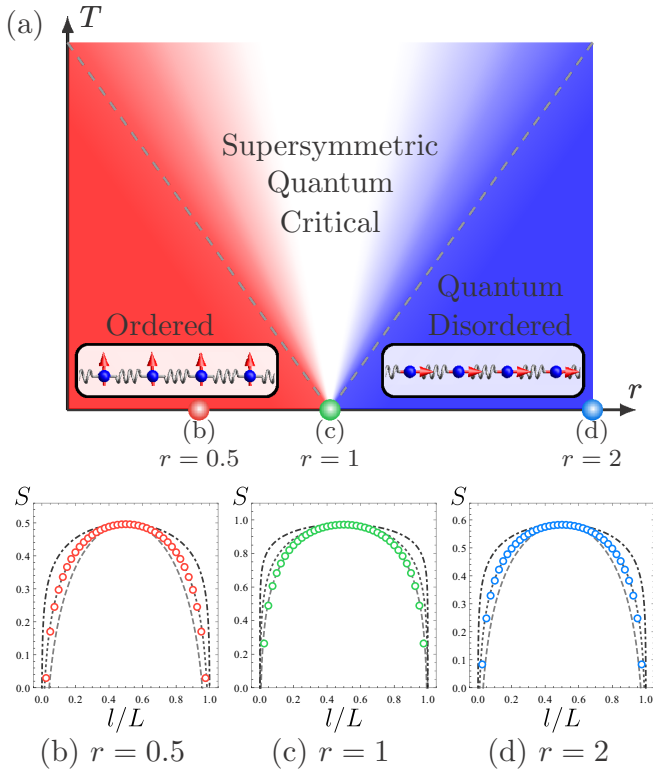


FIG. 2. (a) Phase diagram of the transverse-field Ising model under lattice vibrations. $r < 1$ corresponds to the ordered phase, and the spin degrees of freedom are aligned along the z axis, while $r > 1$ indicates that the system is in the quantum disordered phase and the spin degrees of freedom are along the x axis. $r = 1$ and $T = 0$ are the quantum critical point which is described by the $\mathcal{N} = 1$ supersymmetric conformal field theory (CFT) with central charge $c = 3/2$. (b)–(d) DMRG calculation of the entanglement entropy of the system for three different values of r as indicated in the phase diagram in (a). The values are represented by circles. Here, l is the length of the subsystem. CFT predicts the scaling of entanglement entropy, and the results for central charge $c = 1/2$ (dash-dotted line), $c = 1$ (dotted line), and $c = 3/2$ (dashed line) are plotted as a comparison. At the critical point [in (c)], the scaling suggests a central charge of $3/2$, while away from the critical point [in (b) and (d)], the central charge is 1.

lattice degrees of freedom, whose form is [1,27]

$$\mathcal{S}_0 = \int_{\tau,x} \frac{1}{2} \eta^\top (\partial_\tau + i v_M \sigma_x \partial_x) \eta + \frac{1}{2} (\partial_\tau u)^2 + \frac{v_s^2}{2} (\partial_x u)^2, \quad (3)$$

$$\begin{aligned} \Sigma_M(i\Omega, q) &= g^2 \int_{\partial\Lambda} \frac{d\omega dk}{(2\pi)^2} (ik\sigma_y) G_M(i\omega + i\Omega, k+q) (-ik\sigma_y) G_{\text{ph}}(i\omega, k) = \alpha_g \frac{\rho}{(1+\rho)^2} \sigma_0(i\Omega)\ell - \alpha_g \frac{\rho}{(1+\rho)^2} \sigma_1(v_M k)\ell, \\ \Pi_P(i\Omega, q) &= -\frac{g^2}{2} q^2 \int_{\partial\Lambda} \frac{d\omega dk}{(2\pi)^2} \text{Tr}[\sigma_y G_M(i\omega + i\Omega, k+q) \sigma_y G_M(i\omega, k)] = \alpha_g v_s^2 q^2 \ell, \\ \Gamma_g &= g^2 \int_{\partial\Lambda} \frac{d\omega dk}{(2\pi)^2} \frac{\text{Tr}[(ik\sigma_y) G_M(i\omega, k) \sigma_y G_{\text{ph}}(i\omega, k) (-ik\sigma_y)]}{\text{Tr}[\sigma_y \sigma_y]} G_{\text{ph}}(i\omega, k) = -\alpha_g \frac{\rho}{(1+\rho)} \ell, \end{aligned}$$

where Σ_M and Π_P are self-energies for the Majorana spinor and phonon and Γ_g is the vertex correction to the spin-lattice

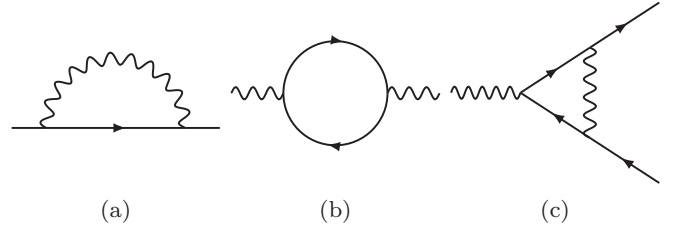


FIG. 3. Feynman diagrams for the RG analysis in the transverse Ising model under lattice vibration up to one-loop order. (a) and (b) are for the fermion and boson self-energies, and (c) is for the vertex correction. The solid line with the arrow and the wavy line stand for the fermion and boson, respectively.

where the Pauli matrices $\sigma_{x,y,z}$ are defined in the two-component Majorana spinor $\eta^\top = (\eta^{(1)} \eta^{(2)})$ space. The Majorana fields are rescaled to have the factor $1/2$, and the shorthand notation $\int_{\tau,x} \equiv \int d\tau dx$ is used hereafter. The two velocities ($v_M = 2Ja$, $v_s = \omega_0 a$) are associated with magnetic exchange and Debye energy scales, respectively.

The two point correlation functions from Eq. (3) are given by

$$\langle \eta_a(\tau, x) \eta_b(0, 0) \rangle = \int \frac{d\omega dk}{(2\pi)^2} G_{M,ab}(i\omega, k) e^{-i\omega\tau + ikx}, \quad (4)$$

$$\langle u(\tau, x) u(0, 0) \rangle = \int \frac{d\omega dk}{(2\pi)^2} G_{\text{ph}}(i\omega, k) e^{-i\omega\tau + ikx}, \quad (5)$$

where $G_M = (-i\omega\sigma_0 - v_M k\sigma_x)^{-1}$ and $G_{\text{ph}} = (\omega^2 + v_s^2 k^2)^{-1}$ are the Majorana and phonon propagators, respectively. The spin-lattice coupling may be identified as (see Appendix A)

$$\mathcal{S}_1 = \frac{g}{2} \int_{\tau,x} (\partial_x u) \eta^\top \sigma_y \eta, \quad (6)$$

with $g = -2\gamma$. The total critical theory, $\mathcal{S}_0 + \mathcal{S}_1$, is analyzed by introducing the two dimensionless coupling constants, $\rho \equiv v_s/v_M$ and $\alpha_g \equiv g^2/(2\pi v_s^2 v_M)$. We perform the RG analysis up to the one-loop order corrections [1,27,29,30]. Only three Feynman diagrams in Fig. 3 are necessary, and the loop corrections are given by

coupling. Note that we parametrize frequency and momentum as $\omega = v_M q \cos \theta$ and $k = q \sin \theta$, so the shell integration

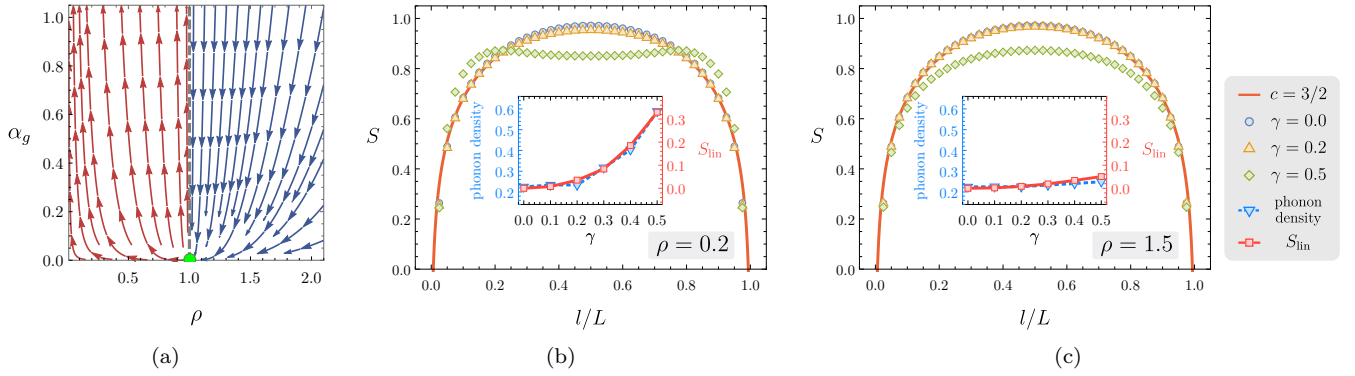


FIG. 4. (a) RG flow diagram with the two dimensionless parameters, the velocity ratio of phonons and spinons ρ ($\equiv v_s/v_M$) and the spin-lattice coupling constant α_g [$\equiv g^2/(2\pi v_s^2 v_M)$]. While the RG flow (red) is directed to $(\rho, \alpha_g) \rightarrow (0, \infty)$ for $\rho < 1$, the flow (blue) is directed to the fixed point $(\rho^*, \alpha_g^*) = (1, 0)$ for $\rho > 1$. The fixed point is described by $\mathcal{N} = 1$ superconformal field theory with central charge $c = 3/2$. (b) and (c) DMRG calculations of the entanglement entropy with spin-lattice coupling γ . The two plots represent each side ($\rho < 1$ and $\rho > 1$) of the flow diagram as $\rho = 0.2$ for (b) and $\rho = 1.5$ for (c). One can observe the strong deviation from the original CFT for $\rho < 1$. The inset shows how the linear entropy and the average phonon occupancy change with γ . The significant increase of the linear entropy for $\rho < 1$ shows the state is flowing away from the fixed point, and a similar trend of phonon density indicates that the phonons are responsible for this.

becomes $\int_{\Lambda} \frac{d\omega dk}{(2\pi)^2} = (v_M/4\pi^2) \int_0^{2\pi} d\theta \int_{\mu}^{\Lambda} q dq$, and $\mu = \Lambda e^{-l}$. After adding the loop corrections to the original action and rescaling and renormalizing the fields and parameters, we get the RG flow equations of the parameters of v_M , v_s , and g as follows:

$$\frac{1}{v_M} \frac{dv_M}{dl} = z - 1 - \alpha_g \frac{2\rho}{(1+\rho)^2}, \quad (7)$$

$$\frac{1}{v_s} \frac{dv_s}{dl} = z - 1 - \frac{\alpha_g}{2}, \quad (8)$$

$$\frac{1}{g} \frac{dg}{dl} = \frac{3}{2}(z-1) - \alpha_g \frac{\rho(2+\rho)}{(1+\rho)^2}. \quad (9)$$

From Eqs. (7)–(9), we obtain the RG flow equations of the dimensionless parameters ρ and α_g ,

$$\frac{d\rho}{dl} = -\frac{\alpha_g}{2} \left(\frac{1-\rho}{1+\rho} \right)^2, \quad \frac{d\alpha_g}{dl} = \alpha_g^2 \left(\frac{1-\rho}{1+\rho} \right). \quad (10)$$

In Fig. 4(a), the flow diagram is illustrated, and the fixed point is at $(\rho^*, \alpha_g^*) = (1, 0)$. The RG flow around the fixed point is intriguing. If the phonon is slower than the Majorana fermion ($\rho < 1$), the fixed point (ρ^*, α_g^*) becomes unstable. In the opposite case where the phonon is faster than the Majorana fermion ($\rho > 1$), the RG flow is directed to the stable fixed point (ρ^*, α_g^*) .

The Hamiltonian at the stable fixed point may be written as

$$H_{sc} = J \sum_i [-s_i^z s_{i+1}^z - s_i^x + p_i^2 + (x_{i+1} - x_i)^2], \quad (11)$$

with rescaled momentum and position operators, $p_j \equiv P_j/\sqrt{M\omega_0}$ and $x_j \equiv \sqrt{M\omega_0} u_j$. We introduce an operator

$$\hat{Q} = - \sum_j \left(\prod_{l < j} s_l^x \right) [(x_{j-1} - x_j) s_j^z + p_j s_j^y] \quad (12)$$

which is fermionic, proven by the Jordan-Wigner transformation, and satisfies $\mathcal{N} = 1$ supersymmetry algebra, $H_{sc} = J\hat{Q}^2$

[31–33] (see Appendix B). Therefore, this fermionic operator becomes a supercharge, $[\hat{Q}, H_{sc}] = 0$, and the $\mathcal{N} = 1$ supersymmetry with central charge $c = 3/2$ is obtained.

A few comments are as follows. First, the supersymmetric quantum state emerges from the spin-lattice coupling. Without the coupling, the state loses supersymmetry unless interactions are fine-tuned. Note that the interactions from the spin lattice are unique in the sense that bosons have a shift symmetry $u_i \rightarrow u_i + a$, in contrast to ladder systems [34–37]. Second, the supersymmetric quantum criticality cannot be obtained by the standard quantum-classical mapping. This is because lattice vibrations are intrinsically tied to spatial dimensions. There are two phonon modes along the two spatial directions, in sharp contrast to one mode in the quantum model. Thus, supersymmetry is intrinsically impossible in the corresponding classical thermal transition. Third, the origin of the supersymmetry in our work is different from the previously suggested ones in the literature [25,26,34,36,38–42] where bosons are made of fermions and special types of interactions or surface degrees of freedom are necessary. In contrast, bosons are from the lattice, and fermions are from the spins in this work. One crucial point is that bosons are in a critical phase in the sense that their spectrum is always gapless, and spin degrees of freedom realize gapless fermionic excitations at the critical point. Last, the $\rho = 1$ fixed line in the RG flow diagram [Fig. 4(a)] is exact up to one loop. Unlike the fixed point at $\alpha_g = 0$, the fixed line for nonzero α_g is not protected by any symmetry and thus may deviate from the straight line when higher-order contributions are included. Nevertheless, we expect the boundary between the stable and unstable regions exists, as predicted in Ref. [37] for a different microscopic model with a similar low-energy theory.

IV. NUMERICAL CALCULATION

Our analysis is further supported by the DMRG method [43–45]. For a chain of length $L = 40$, we calculate the ground state of the system and its bipartite entanglement entropy

for different ratios of energy scales (J, h, γ). We also obtain the central charge of the system utilizing the conformal field theory (CFT) scaling of the entanglement entropy. For an open one-dimensional gapless system of length L , the entanglement entropy S of the ground state scales with the subsystem size l as [46]

$$S = \frac{c}{6} \ln\left(\frac{2L}{\pi} \sin\frac{\pi l}{L}\right) + c', \quad (13)$$

where c is the central charge of the system and c' is a nonuniversal constant. After obtaining the ground state, we can calculate the entanglement entropy by cutting the system at different locations. Comparing the resulting entanglement entropy scaling with the theoretical prediction [Eq. (13)], we determine whether the state is gapless or not and read out the central charge c when it is gapless. In the calculations, we kept up to 500 states to keep the truncation error per step around 10^{-12} .

Without spin-lattice coupling, we find $c = 3/2$ at the critical point ($r = 1$), while $c = 1$ otherwise as the spin sector becomes gapped and only the acoustic phonon contributes [Figs. 2(b)–2(d)]. Two distinct behaviors arise for the regions $\rho > 1$ and $\rho < 1$ when the interaction is turned on and the system is at the critical point. While big deviations from $c = 3/2$ occur for $\rho < 1$ [Fig. 4(b)], the system is stable for $\rho > 1$, manifested by the central charge being unchanged at $c = 3/2$ [Fig. 4(c)]. Thus, our DMRG calculations are consistent with the results of the RG flow. In each calculation, we have computed the linear entropy $S_{\text{lin}} = 1 - \text{Tr} \hat{\rho}_{\text{spin}}^2$ [47,48] with the reduced density matrix of the spin degrees of freedom $\hat{\rho}_{\text{spin}}$ in addition to the average phonon density to measure how strongly the phonons and spins are coupled. It is clear that S_{lin} and phonon density for $\rho = 0.2$ [inset of Fig. 4(b)] demonstrate the conventional decoherence from phonons, which is in contrast to those for $\rho = 1.5$ [inset in Fig. 4(c)], showing that the spins and phonons remain decoupled. Note that for the unstable region $\rho < 1$, the significant deviation from the conformal behavior of the entanglement entropy indicates that a structural transition such as Peierls instability may appear.

A couple of notes on the numerical calculations are as follows. The calculations are done for an open chain with fixed boundary conditions, $u_1 = u_L = 0$. This is to suppress the zero-momentum mode of the acoustic phonon. However, the effect of fixed boundary conditions diminishes as the system size increases, and therefore, we chose an intermediate length of $L = 40$. $L = 40$ is far shorter than the maximum computational ability, even considering the large local Hilbert space (spin-half and boson degrees of freedom), but this is to keep the suppression in effect. As a result, the simulation suffers from finite-size effects (see Appendix D), and the sharp distinction between the two sides near $\rho = 1$ in Fig. 4(a) is not observed in the numerics. Rather, we accept the fact that the finite-size effect is unavoidable while suppressing the zero-momentum mode and observe the qualitative difference between both sides of $\rho < 1$ and $\rho > 1$, but not necessarily near $\rho = 1$.

We also have to truncate the phonon Hilbert space at a certain number of occupancy for the numerical simulation. All calculations are done with the restricted Hilbert space of a maximum of 10 phonons per site. We have checked that this

number is an order larger than the actual phonon occupancies of the calculated ground states and thus the restriction on the Hilbert space does not affect the ground state. Some phonon occupancies in the calculations are shown in the insets in Figs. 4(b) and 4(c). Throughout the calculation, where we scanned the region $0.1 \leq \rho \leq 2.0$ and $0.0 \leq \gamma \leq 0.5$, the phonon occupancies were all below 1.0 except for small ρ and large γ , which is deep in the unstable regime even with the finite-size effect.

V. GENERALIZATION

Our spin chain results may be generalized by considering a generic Landau-Ginzburg Hamiltonian with a local order parameter ϕ [27],

$$H = - \sum_{\langle ij \rangle} t \phi_i \phi_j + \sum_{ijkl} \lambda \phi_i \phi_j \phi_k \phi_l + H_{\text{ph}}. \quad (14)$$

Here, the indices are for the positions of the order parameters. For simplicity, we consider the case where the symmetry group of the order parameter is decoupled from that of the lattice, leaving other cases for future works. The lattice Hamiltonian H_{ph} generally consists of harmonic and anharmonic terms with an additional polarization index. As in the Ising model, we promote the coupling at the lowest order of ϕ to have a spatial modulation to introduce minimal interaction between the order parameter and the lattice vibrations: $t \rightarrow t_{ij} = t + \gamma(u_j - u_i) + O((u_j - u_i)^2)$.

A quantum phase transition may be described by tuning the parameter λ/t . To study the behavior near the phase transition, we again consider the critical field theory. The total action $\mathcal{S} = \mathcal{S}_c + \mathcal{S}_{\text{ph}} + \mathcal{S}_{\text{ph-c}}$ describes the interplay physics between quantum criticality and acoustic phonons, where \mathcal{S}_c is the critical action for the original theory of the order parameter, for instance, $\mathcal{S}_c = \int_{\tau,x} \frac{1}{2}[(\partial_\tau \phi)^2 + (\nabla \phi)^2 + r\phi^2]$ for ϕ^4 theory, \mathcal{S}_{ph} is the action for the acoustic phonons, and $\mathcal{S}_{\text{ph-c}}$ represents the interaction of the two. The coupling term in the action $\mathcal{S}_{\text{ph-c}}$ is solely determined by the symmetry of the theory, and the most relevant interaction term is $\mathcal{S}_{\text{ph-c}} = g \int_{\tau,x} \mathcal{O}_E \sum_{i=1}^d e_{ii}$. The strain tensor $e_{ij} = \partial_i u_j + \partial_j u_i$ with the phonon field u_i is introduced with a spatial dimension d . The form of the energy operator \mathcal{O}_E depends on the system, for example, $\mathcal{O}_E = \phi^2$ in the conventional ϕ^4 theory.

The standard scaling analysis may be performed at the fixed point without the lattice-order parameter coupling. The scaling dimension of the strain tensor $[e_{ij}] = (d+z)/2$ is determined by the phonon action, $[\mathcal{S}_{\text{ph}}] = [\int_{x,\tau} e_{ij}^2]$. The energy operator has the scaling dimension $[\mathcal{O}_E] = z + d - \frac{1}{\nu}$, and the coupling constant g has

$$[g] = \frac{1}{\nu} - \frac{d+z}{2} = \frac{2 - (d+z)\nu}{2\nu}, \quad (15)$$

whose sign becomes the main criterion for the stability. For $[g] < 0$, the quantum criticality of \mathcal{S}_c is stable, so the ground state may be described by a disentangled state of order parameters and phonons. Perturbative calculations give rise to decoherence of quantum states of order parameters. Note that the scaling analysis also applies for a continuous symmetry-broken phase with Goldstone bosons, and it is easy to see that

a lattice coupling is also irrelevant because all the couplings with Goldstone bosons are suppressed [27]. But for $[g] \geq 0$, the disentangled state becomes unstable, indicating two possibilities. First, the second-order phase transition may become a first-order transition as in most thermal phase transitions under lattice vibration. Second, as in the above spin-chain model, a novel quantum criticality may appear. The scaling dimensions of the lattice-order parameter in several models which have $z = 1$ following Eq. (15) are presented in Table I.

Note that our condition becomes the Larkin-Pikin criterion [15] in the limit of classical phase transitions. Namely, setting $z = 0$, $[g] < 0$ becomes the negative heat capacity critical exponent $\alpha = 2 - d\nu < 0$, and the corresponding classical criticality is stable. The generalized Larkin-Pikin criterion may also be applied to unconventional quantum criticalities such as topological phase transitions and deconfined phase transitions (see Appendix C).

VI. DISCUSSION AND CONCLUSION

Decoherence from the environment in a quantum many-body system has been an issue since the start of quantum mechanics and has recently received more attention than ever because of new developments in quantum science and technology. One of the most serious issues in the decoherence is lattice vibration, and experimentalists have fought against this for decades by, for example, cooling the system near zero temperature. Our work provides a different perspective on this fight by showing that phonons may drive the system to a coherent state.

Specifically, the coherent state we find in the spin chain model has the special property of being supersymmetric, and our calculation provides nontrivial predictions in experiments of emergent phenomena in quantum material. The $\mathcal{N} = 1$ supersymmetry indicates that the velocity of acoustic phonons becomes equalized to the spinon velocity, which may be tested by sound attenuation experiments [49,50], for example, in CoNb_2O_6 [51]. The phonon velocity is generically faster than the spinon velocity, so we predict significant decreases of phonon velocity around the quantum critical point, and the two eventually become equal in the ideal case. Thus, we propose that the discovery of supersymmetry is possible by observing the equalized velocities of spinons and phonons in the spin 1/2-chain system. Furthermore, our generalized Larkin-Pikin criterion may become a reliable and useful guideline to look for novel entangled phonon-order parameter systems.

In conclusion, we demonstrated that lattice vibration may be an impetus of a novel quantum many-body state, not an intrinsic source of decoherence. A whole system with spin and lattice degrees of freedom may form a macroscopic quantum many-body state by entangling quantum critical modes and acoustic phonons. One example we discovered in this work is a supersymmetric quantum criticality of an Ising spin chain. Its striking characteristics of the entanglement may be observed in experiments, for example, equal phonon and spinon velocities in the Ising chain. Our results indicate that interplay between quantum criticality and lattice vibration may open a new regime of quantum many-body physics.

ACKNOWLEDGMENTS

We thank P. Coleman, H. Katsura, E. Berg, and S. S. Lee for invaluable discussions and comments. This work was supported by NRF of Korea under Grants No. NRF-2019M3E4A1080411 and No. NRF-2020R1A4A3079707 (S.H., E.G.M.) and NSF-PFC at the JQI (J.L.).

APPENDIX A: SPIN-LATTICE COUPLING IN THE CONTINUUM LIMIT

In the continuum limit, the interaction Hamiltonian H_1 in the main text is written as follows:

$$\begin{aligned} H_1 &= \gamma \sum_i (u_{i+1} - u_i) s_i^z s_{i+1}^z \\ &= -i\gamma \sum_i (u_{i+1} - u_i) \eta_j^{(2)} \eta_{j+1}^{(1)} \\ &\approx -\frac{\gamma}{2} \int dx (\partial_x u) (i\eta^{(2)} \eta^{(1)} - i\eta^{(1)} \eta^{(2)}) \\ &= -\frac{\gamma}{2} \int dx (\partial_x u) (\eta^\top \sigma_y \eta). \end{aligned}$$

After rescaling the Majorana fields, it is written as

$$S_1 = \frac{g}{2} \int_{\tau,x} (\partial_x u) (\eta^\top \sigma_y \eta),$$

where $g = -2\gamma$.

APPENDIX B: SUPERSYMMETRY OF THE (1+1)-DIMENSIONAL TRANSVERSE FIELD ISING MODEL WITH LATTICE VIBRATION

Let us define the following operator:

$$\hat{Q} = - \sum_j \left(\prod_{i<j} s_i^x \right) [(x_{j-1} - x_j) s_j^z + p_j s_j^y],$$

where $x_j \equiv \sqrt{M\omega_0} u_j$ and $p_j \equiv P_j / \sqrt{M\omega_0}$, which are the same in the main text.

First of all, let us check that \hat{Q} is a fermionic operator. To do this, let us consider the following operators:

$$\begin{aligned} \hat{Q}_j^{(1)} &:= -(x_{j-1} - x_j) \left(\prod_{i<j} s_i^x \right) s_j^z, \\ \hat{Q}_j^{(2)} &:= -p_j \left(\prod_{i<j} s_i^x \right) s_j^y. \end{aligned}$$

Then \hat{Q} can be written in terms of $\hat{Q}_j^{(1)}$ and $\hat{Q}_j^{(2)}$, $\hat{Q} = \sum_j (\hat{Q}_j^{(1)} + \hat{Q}_j^{(2)})$. Since $\hat{Q}_j^{(1)}$ and $\hat{Q}_j^{(2)}$ are Hermitian, $(\hat{Q}_j^{(1,2)})^\dagger = \hat{Q}_j^{(1,2)}$, \hat{Q} is Hermitian. They satisfy the following anticommutative relations:

$$\begin{aligned} \{\hat{Q}_i^{(1)}, \hat{Q}_j^{(1)}\} &= 2\delta_{ij}(x_{j-1} - x_j)^2, \\ \{\hat{Q}_i^{(2)}, \hat{Q}_j^{(2)}\} &= 2\delta_{ij}p_j^2, \quad \{\hat{Q}_i^{(1)}, \hat{Q}_j^{(2)}\} = -[\delta_{i,j+1}s_j^z s_{j+1}^z + \delta_{ij}s_j^x], \end{aligned}$$

where we use the properties $[x_i, p_j] = i\delta_{ij}$ and $s_i^a s_j^b = \delta_{ij} \epsilon^{abc} s_j^c + s_j^b s_i^a$. Since $\hat{Q}_j^{(1)}$ and $\hat{Q}_j^{(2)}$ satisfy the anticommutative

relations, they are fermionic operators. Therefore, \hat{Q} is also a fermionic operator because \hat{Q} is the summation of the fermionic operators. From the properties of $\hat{Q}_j^{(1)}$ and $\hat{Q}_j^{(2)}$, we can obtain \hat{Q}^2 ,

$$\begin{aligned}\hat{Q}^2 &= \sum_{i,j} \left[\frac{1}{2} \{ \hat{Q}_i^{(1)}, \hat{Q}_j^{(1)} \} + \frac{1}{2} \{ \hat{Q}_i^{(2)}, \hat{Q}_j^{(2)} \} + \{ \hat{Q}_i^{(1)}, \hat{Q}_j^{(2)} \} \right] \\ &= H_{sc}/J,\end{aligned}$$

where $H_{sc} = J \sum_j [-s_j^z s_{j+1}^x - s_j^x + p_j^2 + (x_{j+1} - x_j)^2]$ is the Hamiltonian at the stable fixed point [Eq. (4) in the main text]. This is (1+1)-dimensional supersymmetry algebra in a lattice [31,32]. And \hat{Q} is Hermitian, $\hat{Q}^\dagger = \hat{Q}$. Also we can easily show $[\hat{Q}, H_{sc}] = 0$. Therefore, \hat{Q} is the supercharge operator for the Hamiltonian.

Some remarks are in order. First, since \hat{Q} is the Hermitian and fermionic operator, it could be represented in terms of Majorana fermions, $\hat{Q} = \sum_j \eta_j^{(1)} (x_{j-1} - x_j) - \sum_j \eta_j^{(2)} p_j$, where $\eta_j^{(1,2)}$ are $\eta_j^{(1)} = -(\prod_{i<j} s_i^x) s_j^z$ and $\eta_j^{(2)} = (\prod_{i<j} s_i^x) s_j^y$, respectively. Second, the supercharge \hat{Q} in the Majorana fermion representation is similar to that in Ref. [32] without $V(\varphi(x))$ and overall sign. Last, there is another choice for the supercharge, $\hat{Q}' = \sum_j (\prod_{i<j} s_i^x) [(x_{j-1} - x_j) s_j^y + p_j s_j^z]$, and in the Majorana fermion representation, $\hat{Q}' = \sum_j \eta_j^{(2)} (x_{j-1} - x_j) - \sum_j \eta_j^{(1)} p_j$, where it satisfies $(\hat{Q}')^2 = H_{sc}/J$, $[\hat{Q}', H_{sc}] = 0$, and $(\hat{Q}')^\dagger = \hat{Q}'$. At the lattice, we need only one of them. However, in the continuum limit, we need both of them [31,32].

APPENDIX C: DISCUSSION OF UNCONVENTIONAL QUANTUM CRITICALITY WITH LATTICE VIBRATIONS

The generalized Larkin-Pikin criterion may also be applied to unconventional quantum criticalities. First, topological phase transitions in weakly correlated systems are generically described by the Dirac/Weyl fermions, whose Hamiltonian is written as $H_{D/W} = \int d^d x \psi^\dagger (-i \partial_a \Gamma^a) \psi$, with $a = 1, \dots, d$, the Clifford algebra matrices Γ_a , and the spinor ψ [52]. The sign of the mass determines whether the system is in the topological phase, and the correlation length critical exponent is $\nu = 1$. Setting $z = 1$, the coupling constant is marginal in $d = 1$ and irrelevant for $d > 1$. For criticalities with $z > 1$, the coupling becomes less irrelevant but is still irrelevant at higher dimensions such as $d = 3$. Thus, a new universality class or instability may appear at $d = 1$, while topological phase transitions in higher dimensions may be decoupled from the lattice vibration.

Second, quantum criticalities with an enlarged symmetry, such as criticalities in a deconfined phase, may have different universality classes from that of the Landau-Ginzburg-Wilson paradigm [53,54]. For example, a Z_2 symmetry-breaking transition with Z_2 local gauge with $d = 2$ has the same universality class as that of the $U(1)$ symmetry transition [55,56], so the lattice vibration becomes decoupled.

Third, the criterion may be applied to the recently proposed quantum annealed criticality [57], which connects a quantum critical point with a line of first-order thermal phase transi-

tions. One good candidate is the Z_4 clock model in $d = 2$. At zero temperature the model shows the $U(1)$ universality class because a fourfold anisotropy is reported to be irrelevant [23,24], but at nonzero temperatures, the model shows nonuniversal behaviors [58]. Namely, its universality class may be the same as that of the Ashkin-Teller (four-state Potts) model with $\nu_{AT} = 2/3$ depending on the systems' parameters [59], indicating a first-order transition.

Last, the criterion indicates that the interplay between lattice vibration and quantum criticality may be accessed perturbatively in recently reported ferroelectric quantum criticalities in SrTiO₃ and KTaO₃ [10–13].

APPENDIX D: DMRG HAMILTONIAN AND THE FINITE-SIZE EFFECT

The Hamiltonian for the transverse-field Ising model with spin-lattice coupling is as follows [Eqs. (3) and (4) in the main text]:

$$\begin{aligned}H &= H_0 + H_1 = \sum_i \left[-J s_i^z s_{i+1}^z - h s_i^x + \frac{P_i^2}{2M} \right. \\ &\quad \left. + \frac{M \omega_0^2}{2} (u_{i+1} - u_i)^2 + \gamma (u_{i+1} - u_i) s_i^z s_{i+1}^z \right].\end{aligned}\quad (D1)$$

We change the basis of the phonons to the *local* boson creation/annihilation operators (b_i/b_i^\dagger) used in Refs. [60,61].

$$u_i = \left(\frac{\hbar^2}{8M^2 \omega_0^2} \right)^{1/4} (b_i^\dagger + b_i). \quad (D2)$$

Let us set $\hbar = M = 1$ from now on. The free phonon part becomes identical to Eq. (5) of Ref. [60],

$$H_{\text{ph}} = \sum_i \sqrt{2} \omega_0 \left(b_i^\dagger b_i + \frac{1}{2} \right) - \frac{\sqrt{2} \omega_0}{4} (b_i^\dagger + b_i) (b_{i+1}^\dagger + b_{i+1}), \quad (D3)$$

and the phonon-spin coupling becomes

$$H_{\text{ph-s}} = \sum_i \frac{\gamma}{(8\omega_0^2)^{1/4}} (b_{i+1}^\dagger + b_{i+1} - b_i^\dagger - b_i) s_i^z s_{i+1}^z. \quad (D4)$$

The Hamiltonian [Eq. (D1)] can be rewritten in the b_i/b_i^\dagger basis as

$$\begin{aligned}H &= \sum_i \left[-J s_i^z s_{i+1}^z - h s_i^x + \sqrt{2} \omega_0 \left(b_i^\dagger b_i + \frac{1}{2} \right) \right. \\ &\quad \left. - \frac{(b_i^\dagger + b_i) (b_{i+1}^\dagger + b_{i+1})}{4} \right) \\ &\quad \left. + \frac{\gamma}{(8\omega_0^2)^{1/4}} (b_{i+1}^\dagger + b_{i+1} - b_i^\dagger - b_i) s_i^z s_{i+1}^z \right].\end{aligned}\quad (D5)$$

With the intermediate system size of $L = 40$ and considering our calculation is in the critical regime, we need to make sure that the qualitative behavior we observe in the numerics is not a result of the finite-size effect. In Figs. 5(a) and 5(b), we plot the size dependence of the $\gamma = 0.5$ entanglement entropies in Figs. 3(b) and 3(c), respectively. As pointed out in the main text, the entanglement entropy scaling

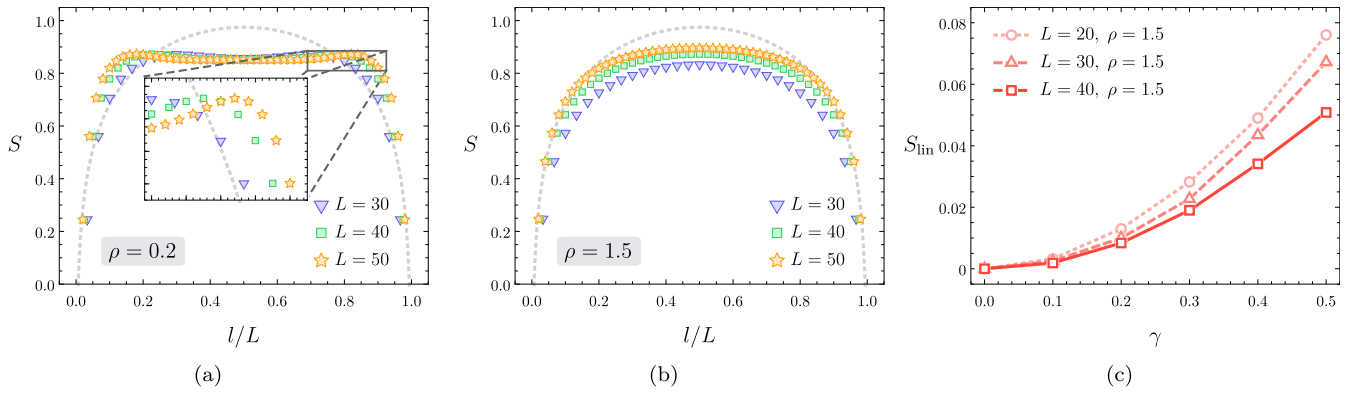


FIG. 5. The finite-size effect of the DMRG calculation. (a) and (b) Entanglement entropy scaling for $\gamma = 0.5$ as shown in Figs. 3 (b) and (c). The deviation from the $c = 3/2$ CFT (gray dashed line) is more prominent for larger systems. (c) Linear entropy as a function of γ as in the inset in Fig. 3(c). The decrease of S_{lin} in system size implies the decoupling of spin and lattice in the thermodynamic limit for this parameter regime ($\rho > 1$).

in the $\rho < 1$ regime [Fig. 3(b)] significantly deviates from the original $c = 3/2$ CFT. The finite-size study shows the deviation is more prominent for larger systems, and this indicates that our conclusion will hold for large enough systems. We also compute the linear entropy, presented in the inset of Fig. 3(c), for a number of system sizes in Fig. 5(c). The nearly zero S_{lin} for $\rho > 1$ demonstrated the spins and lattice

are well decoupled, and the finite-size study shows that S_{lin} approaches zero as we increase the system size. We believe that S_{lin} for $\rho > 1$ will approach zero in the thermodynamic limit as predicted in the field theory calculations. The size dependence of S_{lin} for $\rho < 1$ is less evident than that of $\rho > 1$, which suggests the system will remain unstable for large systems.

-
- [1] S. Sachdev, *Quantum Phase Transitions*, 2nd ed. (Cambridge University Press, Cambridge, 2011).
- [2] P. Coleman and A. J. Schofield, *Nature (London)* **433**, 226 (2005).
- [3] S. Sachdev and B. Keimer, *Phys. Today* **64**(2), 29 (2011).
- [4] X. Wan, A. M. Turner, A. Vishwanath, and S. Y. Savrasov, *Phys. Rev. B* **83**, 205101 (2011).
- [5] P. Hosur, S. A. Parameswaran, and A. Vishwanath, *Phys. Rev. Lett.* **108**, 046602 (2012).
- [6] T. Kondo *et al.*, *Nat. Commun.* **6**, 10042 (2015).
- [7] E.-G. Moon, C. Xu, Y. B. Kim, and L. Balents, *Phys. Rev. Lett.* **111**, 206401 (2013).
- [8] S. A. Yang, H. Pan, and F. Zhang, *Phys. Rev. Lett.* **113**, 046401 (2014).
- [9] S. E. Han, G. Y. Cho, and E.-G. Moon, *Phys. Rev. B* **95**, 094502 (2017).
- [10] S. E. Rowley, L. J. Spalek, R. P. Smith, M. P. M. Dean, M. Itoh, J. F. Scott, G. G. Lonzarich, and S. S. Saxena, *Nat. Phys.* **10**, 367 (2014).
- [11] K. Ahadi, L. Galletti, Y. Li, S. Salmani-Rezaie, W. Wu, and S. Stemmer, *Sci. Adv.* **5**, eaaw0120 (2019).
- [12] T. F. Nova, A. S. Disa, M. Fechner, and A. Cavalleri, *Science* **364**, 1075 (2019).
- [13] X. Li, T. Qiu, J. Zhang, E. Baldini, J. Lu, A. M. Rappe, and K. A. Nelson, *Science* **364**, 1079 (2019).
- [14] P. Chandra, P. Coleman, M. A. Continentino, and G. G. Lonzarich, *arXiv:2012.01601*.
- [15] A. I. Larkin and S. A. Pikin, *Sov. Phys. JETP* **29**, 891 (1969).
- [16] D. J. Bergman and B. I. Halperin, *Phys. Rev. B* **13**, 2145 (1976).
- [17] M. A. de Moura, T. C. Lubensky, Y. Imry, and A. Aharony, *Phys. Rev. B* **13**, 2176 (1976).
- [18] J. Sak, *Phys. Rev. B* **10**, 3957 (1974).
- [19] J. Bruno and J. Sak, *Phys. Rev. B* **22**, 3302 (1980).
- [20] F. J. Wegner, *J. Phys. C* **7**, 2109 (1974).
- [21] P. Di Francesco, P. Mathieu, and D. Sénéchal, *Conformal Field Theory* (Springer, New York, 1997).
- [22] J. Tobochnik, *Phys. Rev. B* **26**, 6201 (1982).
- [23] A. Pelissetto and E. Vicari, *Phys. Rep.* **368**, 549 (2002).
- [24] M. Hasenbusch and E. Vicari, *Phys. Rev. B* **84**, 125136 (2011).
- [25] W. Witzczak-Krempa and J. Maciejko, *Phys. Rev. Lett.* **116**, 100402 (2016).
- [26] S.-K. Jian, C.-H. Lin, J. Maciejko, and H. Yao, *Phys. Rev. Lett.* **118**, 166802 (2017).
- [27] A. Altland and B. D. Simons, *Condensed Matter Field Theory*, 2nd ed. (Cambridge University Press, Cambridge, 2010).
- [28] N. Ishimura, *J. Phys. Soc. Jpn.* **53**, 1472 (1984).
- [29] I. Herbut, *A Modern Approach to Critical Phenomena* (Cambridge University Press, Cambridge, 2007).
- [30] R. Shankar, *Quantum Field Theory and Condensed Matter: An Introduction* (Cambridge University Press, Cambridge, 2017).
- [31] V. Rittenberg and S. Yankielowicz, CERN, Technical Report No. CERN-TH-3263, 1982 (unpublished).
- [32] S. Elitzur, E. Rabinovici, and A. Schwimmer, *Phys. Lett. B* **119**, 165 (1982).
- [33] K. Hori, S. Katz, and A. Klemm, *Mirror Symmetry*, Clay Mathematics Monographs (American Mathematical Society, Providence, RI, 2003).

- [34] L. Huijse, B. Bauer, and E. Berg, *Phys. Rev. Lett.* **114**, 090404 (2015).
- [35] M. Sittte, A. Rosch, J. S. Meyer, K. A. Matveev, and M. Garst, *Phys. Rev. Lett.* **102**, 176404 (2009).
- [36] B. Bauer, L. Huijse, E. Berg, M. Troyer, and K. Schoutens, *Phys. Rev. B* **87**, 165145 (2013).
- [37] O. Alibert, J. Ruhman, E. Berg, and E. Altman, *Phys. Rev. B* **95**, 075132 (2017).
- [38] S.-S. Lee, *Phys. Rev. B* **76**, 075103 (2007).
- [39] T. Grover, D. N. Sheng, and A. Vishwanath, *Science* **344**, 280 (2014).
- [40] P. Ponte and S.-S. Lee, *New J. Phys.* **16**, 013044 (2014).
- [41] S.-K. Jian, Y.-F. Jiang, and H. Yao, *Phys. Rev. Lett.* **114**, 237001 (2015).
- [42] S. Saha, E. J. König, J. Lee, and J. H. Pixley, *Phys. Rev. Research* **2**, 013252 (2020).
- [43] U. Schollwöck, *Rev. Mod. Phys.* **77**, 259 (2005).
- [44] G. K.-L. Chan and S. Sharma, *Annu. Rev. Phys. Chem.* **62**, 465 (2011).
- [45] ITENSOR C++ library, version 3.0, <http://itensor.org/>.
- [46] P. Calabrese and J. Cardy, *J. Stat. Mech.* (2004) P06002.
- [47] W. H. Zurek, S. Habib, and J. P. Paz, *Phys. Rev. Lett.* **70**, 1187 (1993).
- [48] C. H. Bennett, H. J. Bernstein, S. Popescu, and B. Schumacher, *Phys. Rev. A* **53**, 2046 (1996).
- [49] H. Yamaguchi, S. Yasin, S. Zherlitsyn, K. Omura, S. Kimura, S. Yoshii, K. Okunishi, Z. He, T. Taniyama, M. Itoh, and M. Hagiwara, *J. Phys. Soc. Jpn.* **80**, 033701 (2011).
- [50] Z. Wang, T. Lorenz, D. I. Gorbunov, P. T. Cong, Y. Kohama, S. Niesen, O. Breunig, J. Engelmayer, A. Herman, J. Wu, K. Kindo, J. Wosnitza, S. Zherlitsyn, and A. Loidl, *Phys. Rev. Lett.* **120**, 207205 (2018).
- [51] R. Coldea, D. A. Tennant, E. M. Wheeler, E. Wawrzynska, D. Prabhakaran, M. Telling, K. Habicht, P. Smeibidl, and K. Kiefer, *Science* **327**, 177 (2010).
- [52] N. P. Armitage, E. J. Mele, and A. Vishwanath, *Rev. Mod. Phys.* **90**, 015001 (2018).
- [53] T. Senthil, A. Vishwanath, L. Balents, S. Sachdev, and M. P. A. Fisher, *Science* **303**, 1490 (2004).
- [54] C. Wang, A. Nahum, M. A. Metlitski, C. Xu, and T. Senthil, *Phys. Rev. X* **7**, 031051 (2017).
- [55] S. Sachdev, *Rep. Prog. Phys.* **82**, 014001 (2018).
- [56] E.-G. Moon, [arXiv:1812.05621](https://arxiv.org/abs/1812.05621).
- [57] P. Chandra, P. Coleman, M. A. Continentino, and G. G. Lonzarich, [arXiv:1805.11771](https://arxiv.org/abs/1805.11771).
- [58] A. Taroni, S. T. Bramwell, and P. C. W. Holdsworth, *J. Phys.: Condens. Matter* **20**, 275233 (2008).
- [59] L. P. Kadanoff, *Ann. Phys. (NY)* **120**, 39 (1979).
- [60] L. G. Caron and S. Moukouri, *Phys. Rev. B* **56**, R8471(R) (1997).
- [61] W. Barford and R. J. Bursill, *Phys. Rev. Lett.* **95**, 137207 (2005).